Theoretical analysis of the Auger mechanism in a GaInAsSb infrared photovoltaic detector

Yuan Tian
Tianming Zhou
Baolin Zhang
Yixin Jin
Yongqiang Ning
Hong Jiang
Guang Yuan
Chinese Academy of Sciences
Changchun Institute of Physics
Changchun 130021, China
E-mail: snmocvd@public.cc.jl.cn

Abstract. A theoretical analysis of the Auger mechanism in a GaInAsSb infrared photovoltaic detector is reported. The considerations are carried out for near-room temperature and 2.5-μm wavelength. The results show that the Auger mechanism can be suppressed by optimizing the material parameters. Thus, the performance of such detectors can be improved.
[S0091-3286(98)02206-5]

Subject terms: Auger mechanism; GaInAsSb infrared photovoltaic detector; R_0A product; detectivity.

Paper 12097 received Sep. 8, 1997; revised manuscript received Jan. 29, 1998; accepted for publication Jan. 30, 1998.

1 Introduction

In recent years, the direct-narrow-bandgap GaInAsSb quaternary alloys—whose wavelength, ranging from 0.87 to 12 μm, covers three important infrared wavelength ranges (2 to 4, 3 to 5, and 8 to 12 μm)—have become very important materials for the fabrication of detectors designed for infrared-wavelength application.[1,2] GaInAsSb quaternary alloys lattice-matched to GaSb are potentially useful materials for detectors in the 2- to 4-μm wavelength range.[3,4] For example, a GaInAsSb/GaSb infrared detector at wavelengths from 1.7 to 2.4 μm has been prepared.[5]

However, no theoretical analysis of the GaInAsSb detector has been reported so far. In this paper, theoretical calculation and analysis results for a $Ga_{0.8}In_{0.2}As_{0.19}Sb_{0.81}$ infrared photovoltaic (IR PV) detector, whose wavelength is 2.5 μm with a 300-K operating temperature, are reported.

Among noise mechanisms in narrow-bandgap materials, the Auger mechanism is the most important mechanism for the performance of an IR PV detector working near room temperature.[6,7] Therefore, we consider the effect of the Auger mechanism on a GaInAsSb homojunction detector lattice-matched to GaSb.

2 Detector Structure and Theoretical Analysis

The detector structure of n-$Ga_xIn_{1-x}As_{1-y}Sb_y$/p-$Ga_xIn_{1-x}As_{1-y}Sb_y$/GaSb is shown in Fig. 1. Because it is required that the GaInAsSb quaternary alloys be lattice-matched to GaSb, the composition x is related to the composition y by

$$y=\frac{0.408x+0.022}{0.009x+0.421}, \tag{1}$$

where the GaInAsSb lattice constant is gotten by a linear interpolation method (see the appendix). In the following, we only give the calculation results for the composition x at 0.8, at which the corresponding composition y is 0.81.

The figure of merit usually used to characterize the sensitivity of IR PV detectors is the detectivity D^*, which depends on the quantum efficiency and the zero-bias resistance–junction-area (R_0A) product,[8]

$$D^*=\frac{\lambda\eta q}{hc}\left(\frac{R_0A}{4KT}\right)^{1/2}. \tag{2}$$

In the following calculation, several assumptions are made:

1. Infrared radiation of wavelength λ shorter than the cutoff wavelength λ_c is absorbed by the detector and produces electron-hole pairs, which produce the diffusion current. When we assume $\lambda=\lambda_c=hc/E_g$, Eq. (2) can be expressed by
$$D^*=\frac{\eta q}{Eg}\left(\frac{R_0A}{4KT}\right)^{1/2}. \tag{3}$$
2. The quantum efficiency η is 100%; thus Eq. 3 is further simplified to
$$D^*=\frac{q}{Eg}\left(\frac{R_0A}{4KT}\right)^{1/2}. \tag{4}$$

When the temperature and the compositions x and y are fixed, the energy bandgap E_g is also fixed, so that the detectivity is only related to the R_0A product.

We consider the diffusion current only in a low-injection case, in which the diffusion current is due to the minority carriers. Then the R_0A products in the n and p regions are given respectively by[9]

$$(R_0A)_e=\frac{KT}{q^2}\frac{D_ep}{L_en_i^2}\frac{r_e\sinh\delta+\cosh\delta}{\cosh\delta+\sinh\delta} \quad (p \text{ region}), \tag{5}$$

$$(R_0A)_p=\frac{KT}{q^2}\frac{D_pn}{L_pn_i^2}\frac{r_p\sinh\theta+\cosh\theta}{r_p\cosh\theta+\sinh\theta} \quad (n \text{ region}) \tag{6}$$

 0091-3286/98/$10.00

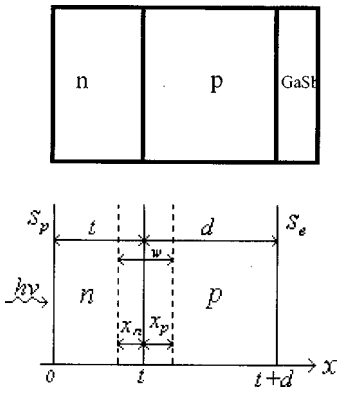

Fig. 1 Simplified structure of a detector: t, n-region width; d, p-region width; w, width of depletion region; x_n, width of depletion region on n side; x_p, width of depletion region on p side.

$$D_i=\frac{KT}{q}\mu_i, \quad L_i=(D_i\tau_i)^{1/2}, \quad \gamma_i=\frac{L_iS_i}{D_i} \quad (i=n \text{ or } p),$$

$$\delta=\frac{1}{L_e}\left(d-\frac{n}{n+p}w\right), \quad \theta=\frac{1}{L_p}\left(t-\frac{p}{n+p}w\right)$$

where

D_i = diffusion coefficient (cm^2/s) for holes in n region or for electrons in p region

L_i = diffusion length (cm) for holes in n region or for electrons in p region

μ_i = effective mobility ($cm^2/V\,s$) for holes in n region or for electrons in p region

S_i = surface recombination velocity (m/s) for holes in n region or for electrons in p region

τ_i = carrier lifetime (s) for hole in n region or for electron in p region

q = electronic charge (C)

T = detector temperature (K)

k = Boltzmann's constant

n,p = major-carrier concentrations (cm^{-3}) in n region and p region, respectively

n_i = intrinsic carrier concentration (cm^{-3}).

These relations are fulfilled for the one-dimensional detector model with an abrupt junction where a spatial charge of width w surrounds the metallographic junction boundary $x=t$, and two quasineutral regions $(0,t-x_n)$ and $(t+x_p,d-x_p)$ are homogeneously doped.

The diffusion current contributions from the n and p regions are added to give the total diffusion current, and the total R_0A product from both sides is[10]

$$\frac{1}{(R_0A)_{\text{total}}}=\frac{1}{(R_0A)_e}+\frac{1}{(R_0A)_p}. \tag{7}$$

In Eqs. (5) and (6), the R_0A products are incorporated in the minority-carrier lifetime, determined by the Auger mechanism.

Among the ten different types of Auger processes that are possible in an InSb-like band structure, the two with the smallest threshold energy—Auger 1 (A-1) and Auger 7 (A-7)—are the ones of practical importance.[11–13] Because the band structure of the GaInAsSb quaternary alloys is complicated, it is simplified to an InSb-like band structure in this paper. In narrow-bandgap materials, when the spin-split-off band has width near to or wider than the energy bandgap E_g, the spin-split-off band plays a much more important role than A-7 in the Auger mechanism for direct-bandgap materials, and the resulting process is called Auger S (A-S). For $Ga_{0.8}In_{0.2}As_{0.19}Sb_{0.81}$ at 300 K, the width of the spin-split-off band is 0.605 eV, while the energy bandgap is 0.494 eV (see the appendix), so we include A-S in the calculation. The A-1 mechanism is dominant in n-type materials, while A-7 and A-S are dominant in p-type.[14,15] The carrier lifetime associated with the Auger mechanism determines the performance of most near-room-temperature PV detectors.

The effective carrier lifetime can be determined by[16]

$$\frac{1}{\tau_A}=\frac{1}{\tau_{\text{A-1}}}+\frac{1}{\tau_{\text{A-7}}}+\frac{1}{\tau_{\text{A-S}}}. \tag{8}$$

The lifetimes for the A-1, A-7, and A-S mechanisms are written respectively as[16]

$$\tau_{\text{A-1}}=\frac{2\tau^i_{\text{A-1}}}{1+n_0/p_0}, \tag{9}$$

$$\tau_{\text{A-7}}=\frac{2\tau^i_{\text{A-7}}}{1+p_0/n_0}, \tag{10}$$

$$\tau_{\text{A-S}}=\frac{2\tau^i_{\text{A-S}}}{1+p_0/n_0}, \tag{11}$$

where p_0 and n_0 are the hole and electron carrier concentration at equilibrium state in the same material, and τ^i indicates the intrinsic recombination time.

The intrinsic A-1 recombination lifetime is given by[12]

$$\tau^i_{\text{A-1}}=\frac{3.8\times10^{-18}\epsilon_s(1+\mu)^{1/2}(1+2\mu)\exp\left(\frac{1+2\mu}{1+\mu}\frac{E_g}{KT}\right)}{\frac{m_e^*}{m_0}|F_1F_2|^2\left(\frac{KT}{E_g}\right)^{3/2}}, \tag{12}$$

where

$\mu=m_e^*/m_h^*$ = ratio of the conduction-band to the heavy-hole valence-band effective mass

ϵ_S = relative static dielectric constant

m_0 = electron static mass

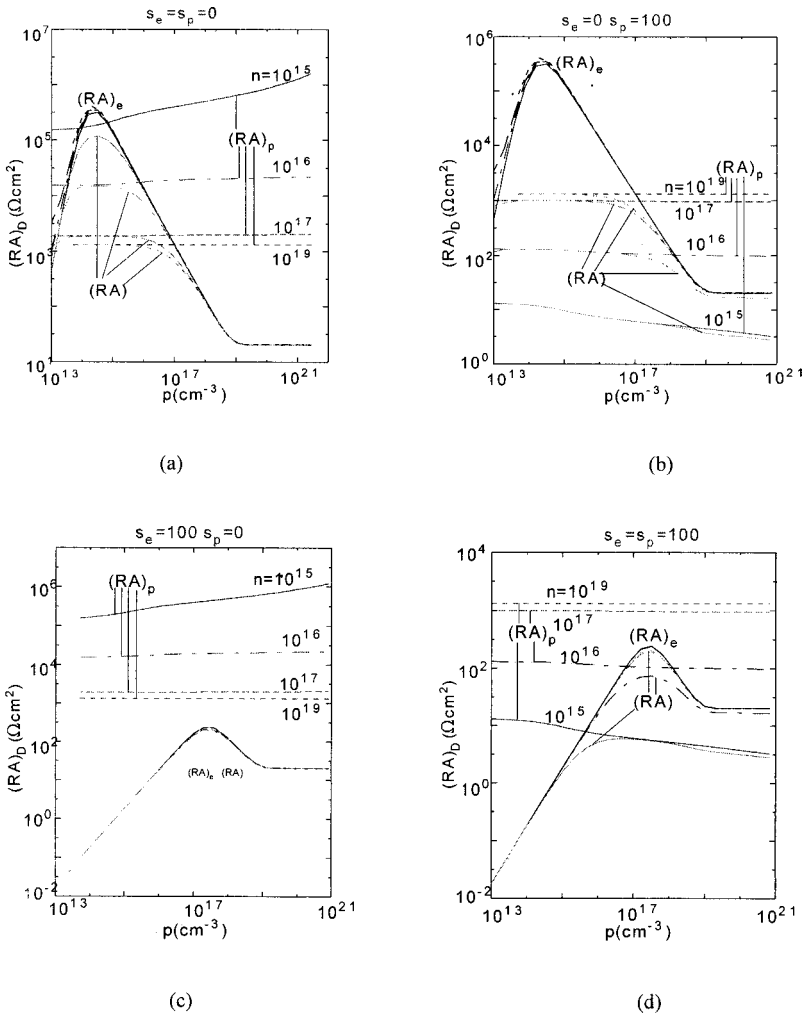

Fig. 2 The calculated R_0A product as a function of the p-side carrier concentration for a GaInAsSb PV detector operated at 300 K and 2.5-μm wavelength; $d=5\ \mu$m, $t=1\ \mu$m, $\mu_p=240$ cm^2/V s, $\mu_e=2900$ cm^2/V s.

F_1, F_2 = overlap integrals of the periodic part of the electron wave function.

The intrinsic A-7 recombination time is given by[12]

$$\tau^i_{\text{A-7}}=\gamma\tau^i_{\text{A-1}}, \tag{13}$$

where γ is the ratio of the A-7 to the A-1 intrinsic recombination time. According to Ref. 12,

$$\gamma=2\frac{m^*_e(E_{\text{th}})}{m^*_{e0}}\frac{1-5E_g/4KT}{1-3E_g/2KT}. \tag{14}$$

The intrinsic A-S recombination time is calculated using theory described in Ref. 17:

$$\tau^i_{\text{A-S}}=\frac{5\epsilon m^3_{hh}m^{*3/2}_e KT\Delta^2(Eg+\Delta)\exp(\Delta-E_g/KT)}{54\pi^4 n_i^2 e^4\hbar^3 m^{*5/2}_s(\Delta-E_g)}. \tag{15}$$

3 Calculation Results

The calculations have been performed for an np $Ga_{0.8}In_{0.2}As_{0.19}Sb_{0.81}$ PV detector operated at 300 K and 2.5-μm wavelength. The dependence of the material parameters of GaInAsSb alloys that are needed for calculating the compositions x and y is given in the appendix.

3.1 R_0A Product

Figure 2 shows the R_0A products in the n and p regions and their sum as functions of the carrier concentrations in those regions, for various values of the illuminated-surface recombination velocity S_p and back-surface recombination velocity S_e, where the widths in the p and n regions are 5 and 1 μm, respectively, and the mobilities μ_p and μ_n are 240 and 2900 cm^2/V s, respectively. These results are gotten through Eqs. (5), (6), and (7).

First, the R_0A product in the p region, $(R_0A)_e$, is analyzed.

1. A similar situation exists in the four parts of Fig. 2, in

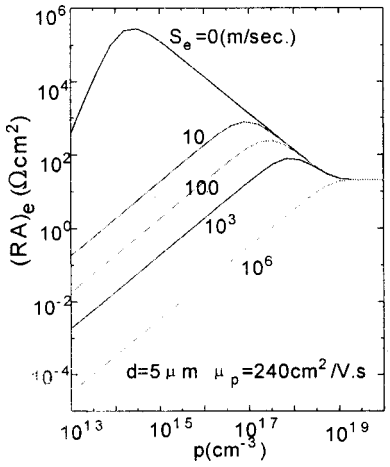

Fig. 3 The effect of the back-surface recombination velocity on the $(R_0A)_e$ product.

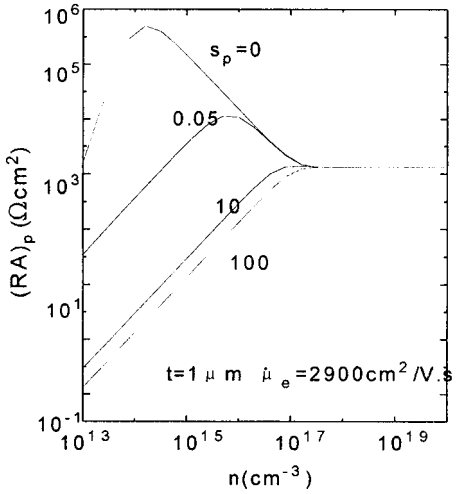

Fig. 4 The effect of the illuminated-surface recombination velocity on the $(R_0A)_p$ product.

that increasing the carrier concentration in the n region will not affect $(R_0A)_e$. Thus, Eq. (5) can be approximated by

$$(R_0A)_e=\frac{KT}{q^2}\frac{D_e p}{L_e n_i^2}\frac{r_e\sinh(d/L_e)+\cosh(d/L_e)}{r_e\cosh(d/L_e)+\sinh(d/L_e)}. \quad (16)$$

2. When the back-surface recombination velocity is not equal to 0 [see Fig. 2(c) and 2(d)] and the n-side carrier concentration is larger than 10^{17} cm^{-3}, the $(R_0A)_{\text{total}}$ product is almost entirely due to the $(R_0A)_e$ product: $(R_0A)_{\text{total}}=(R_0A)_e$. Under this condition the n-side carrier concentration is larger than the p-side carrier concentration, and the structure is called the n^+p structure. In general, the n^+p structure requires a carrier concentration in the n region larger than 10^{21} cm^{-3} and a width less than 1 μm. We discuss the n^+p structure later.
3. As the back-surface recombination velocity increases from 0 to 100 m/s, the $(R_0A)_e$ product decreases by nearly three orders of magnitude, and the peak of the $(R_0A)_e$ product is moved to the direction in which the p-side carrier concentration increases. Figure 3 shows the explanation. On increasing back-surface recombination velocity, the peak of the $(R_0A)_e$ product will clearly decrease and move in the direction of the larger p-side carrier concentration. At $S_e=10^6$ m/s, the peak of the $(R_0A)_e$ product disappears.

Secondly, let us consider the $(R_0A)_p$ product in the n region.

1. When the carrier concentration in the n region is larger than 10^{16} cm^{-3}, the $(R_0A)_p$ product will be independent of the carrier concentration in the p region. Thus, Eq. (6) can be approximated as follows:

$$(R_0A)_p=\frac{KT}{q}\frac{D_p n}{L_p n_i^2}\frac{r_p\sinh(t/L_p)+\cosh(t/L_p)}{r_p\cosh(t/L_p)+\sinh(t/L_p)}. \quad (17)$$

2. When the illuminated-surface recombination velocity is equal to 100 m/s [see Fig. 2(b) and 2(d)] and the carrier concentration in the n region is less than 10^{15} cm^{-3}, the $(R_0A)_{\text{total}}$ product can be expressed by $(R_0A)_{\text{total}}=(R_0A)_p$, in which the carrier concentration in the p region is in the range of 10^{17} to 10^{18} cm^{-3}. Because the intrinsic carrier concentration in $Ga_{0.8}In_{0.2}As_{0.19}Sb_{0.81}$ material is near 10^{14} cm^{-3}, the np structure can be treated as an $i(n^-)$-p structure. If n-type material is grown in front of the $i(n^-)$-p structure, the detector structure becomes an n-(i)-p structure and thus effectively suppresses the Auger process. Such a device is called an extracting detector.[18,19]
3. When the illuminated-surface recombination velocity is equal to zero [see Fig. 2(a) and 2(c)], the $(R_0A)_p$ product will decrease with increasing n-side carrier concentration, whereas the contrary occurs when the illuminated-surface recombination velocity is equal to 100 m/s [see Fig. 2(b) and 2(d)]. This phenomenon is explained in Fig. 4, which shows the effect of different illuminated-surface recombination velocities on the $(R_0A)_p$ product. The results in Fig. 4 are similar to those in Fig. 3.

From Fig. 3 and Fig. 4, we can see whether the back-surface recombination velocity or the illuminated-surface recombination velocity will seriously affect the performance of a GaInAsSb detector.

In the following, we discuss the influence of material parameters on the detectivity for different detector structures. The practical working limit for most IR detectors is background-limited photodetection (BLIP), in which optical generation resulting from thermal background radiation exceeds the thermal component. The BLIP detectivity depends only on the temperature and incident optical wavelength. For a $Ga_{0.8}In_{0.2}As_{0.19}Sb_{0.81}$ IR PV detector working at 300 K and 2.5-μm wavelength, the BLIP detectivity reaches 4.96×10^{12} cm Hz$^{1/2}$/W.

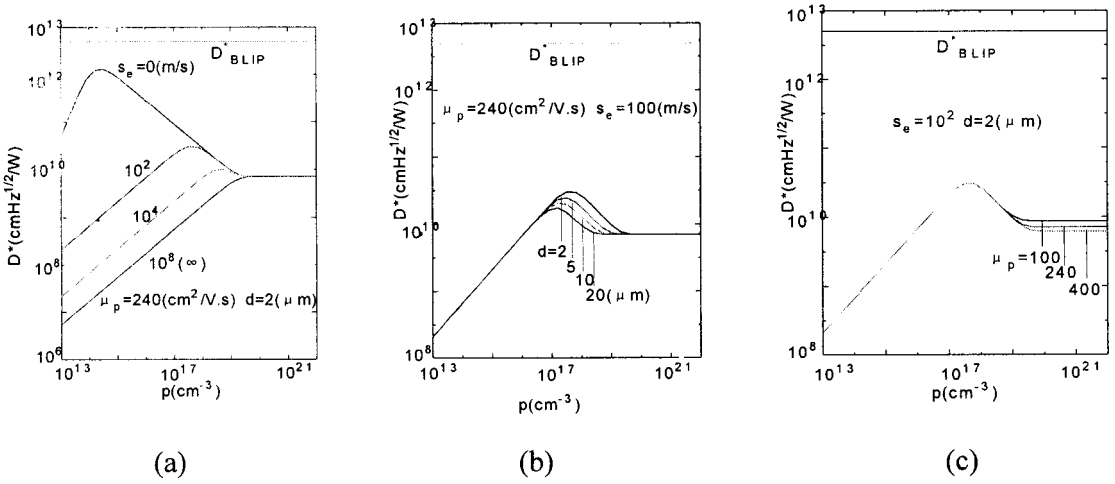

Fig. 5 The calculated detectivity of a GaInAsSb PV detector operated in an n^+p structure as a function of the p-side carrier concentration p and (a) the back-surface recombination velocity S_e; (b) the p-side width d; (c) the p-side mobility μ_p. The BLIP detectivity has been calculated for $T_B = 300$ K and $\eta = 1$.

3.2 *An n^+p-Structure Detector*

The realization of $Ga_xIn_{1-x}As_{1-y}Sb_y$ PV detectors is usually based on an n^+p structure. For that structure, the junction resistance is limited only by diffusion of the minority carrier from the p side into the depletion region.[18] The above discussion indicates that the n-p structure can be regarded as an n^+p structure if the back-surface recombination velocity is not equal to zero. Figure 5 shows the dependence of the detectivity for an n^+p-structure detector on the material parameters in the p region, such as the width d, the mobility μ_p, and the back-surface recombination velocity S_e.

The effect of the back-surface recombination velocity on the R_0A product has been discussed. Because $D^* \propto [(R_0A)_{\text{total}}]^{1/2}$ [Eq. (2)], it is an inevitable outcome that the back-surface recombination velocity will have an effect on the detectivity.

A common characteristic exists in each of parts of Fig. 5. When the p-side carrier concentration is larger than 10^{20} cm^{-3}, the detectivity remains constant on increasing the p-side carrier concentration without variation of the other parameters.

The dependence of the detectivity on the p-side carrier concentration can be divided into three regions. In the range of $p < 10^{16}$ cm^{-3}, only the variation of the back-surface recombination velocity will have an effect on the detectivity; in the range of $p > 10^{20}$ cm^{-3}, only the p-side mobility will have an influence on the detectivity. In the p-side carrier concentration range of 10^{16} to 10^{20} cm^{-3}, all of parameters will affect the detectivity. Now, let us analyze the above results.

The electron diffusion length in the p region is related to the p-side carrier concentration. Table 1 shows the relationship. In view of Table 1, we subject Eq. (16) to a further approximation on the basis of the relationship between L_e and d: For $d \gg L_e$ ($p > 10^{20}$ cm^{-3}),

$$(R_0A)_e = \frac{KTp\tau_e}{q^2 n_i^2 L_e}. \tag{18}$$

For $d \ll L_e$ ($p < 10^{16}$ cm^{-3}),

$$(R_0A)_e = \frac{KTp}{q^2 n_i^2}\frac{L_e}{D_e}\frac{r_e d/L_e + 1}{r_e + d/L_e} \tag{19}$$

if d/L_e is neglected in Eq. (19),

$$(R_0A)_e = \frac{KTp}{q^2 n_i^2 s_e}. \tag{20}$$

For $d \sim L_e$($10^{16} < p < 10^{20}$ cm^{-3}), one must use Eq. (16) itself.

Equations (20), (18), and (16) correspond to the three regions mentioned. For $d \ll L_e$, the $(R_0A)_e$ product is independent of the width and the mobility, whereas for $d \gg L_e$ the $(R_0A)_e$ product is independent of S_e and d.

These results show that reducing the volume and decreasing the mobility in the p region will increase the corresponding detectivity. Under the condition of thin p region ($d \ll L_e$), the lower surface recombination velocity will improve the detectivity.

Table 1 The relation of the electron diffusion length to the p-side carrier concentration.

p-Side carrier concentration p (cm^{-3})	Electron diffusion length in p region, L_e (μm)
$p < 10^{16}$	$L_e > 10^2$
$10^{16} < p < 10^{20}$	$10^{-2} < L_e < 10^2$
$p > 10^{20}$	$L_e < 10^{-2}$

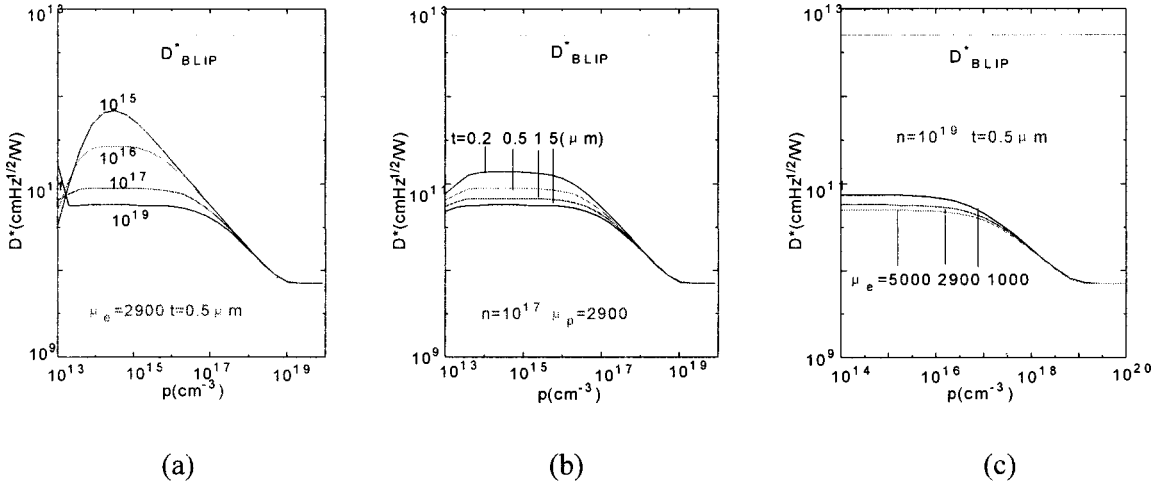

Fig. 6 The calculated detectivity of a GaInAsSb PV detector operated in an *np* structure as a function of the *p*-side carrier concentration *p* and (a) the *n*-side carrier concentration *n*; (b) the *n*-side width *t*; (c) the *n*-side mobility μ_p. In the condition of $S_e = S_p = 0$, $\mu_p = 240$ cm^2/V s, and $d = 5$ μm, the BLIP detectivity has been calculated for $T_B = 300$ K and $\eta = 1$.

3.3 *An np-Structure Detector*

3.3.1 $S_e = S_p = 0$

Figure 6 shows the effect of the *n*-side parameters on the detectivity at $S_e = S_p = 0$; the results correspond to those in Fig. 2(a). Because $(R_0A)_{\text{total}} = (R_0A)_p$ in the range of $p < 10^{16}$ cm^{-3}, the influence of the *n*-side parameters on the detectivity takes place mainly in this range. In contrast, the detectivity is mainly affected by the *p*-side parameters in the range of $p > 10^{19}$ cm^{-3}, as is shown in Fig. 7. In the range of $10^{16} < p < 10^{19}$ cm^{-3}, regardless of the parameter values in the *n* region or those in the *p* region, all of them will affect the detectivity.

3.3.2 $S_e = 0$, $S_p = 100$ m/s

Figure 8 shows the influence of the *n*-side parameters on the detectivity at $S_e = 0$ and $S_p = 100$ m/s. The situation differs from that with $S_p = 0$ in two ways: the greater the width and the larger the carrier concentration, the higher is the detectivity. The influence of the *p*-side parameters on the detectivity is similar to that at $S_e = S_p = 0$; we do not show the results here.

4 Conclusions

Calculation and analysis of the effect of material parameters of a $Ga_{0.8}In_{0.2}As_{0.19}Sb_{0.81}$ IR PV detector on the R_0A product and the detectivity at 300 K have been worked out. It has been shown that:

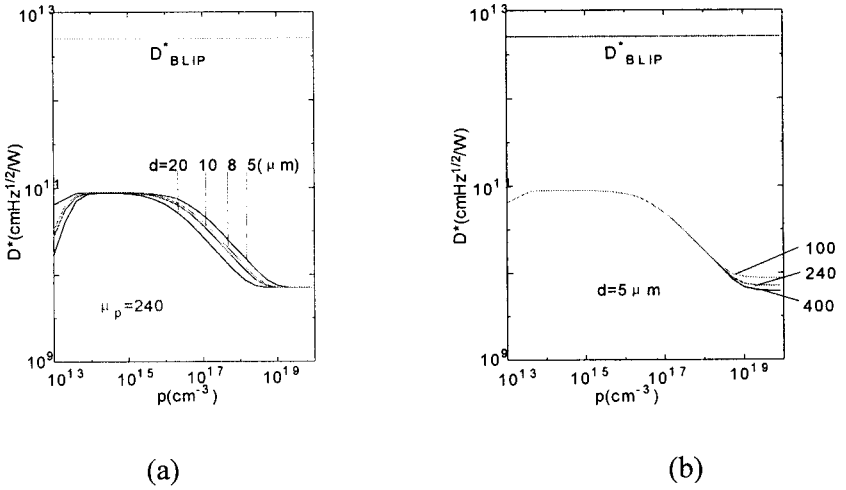

Fig. 7 The calculated detectivity of a GaInAsSb PV detector operated in an *np* stucture as a function of the *p*-side carrier concentration *p* and (a) the *p*-side width *d*; (b) the *p*-side mobility μ_p. In the condition of $S_e = S_p = 0$, $n = 10^{17}$ cm^{-3}, and $t = 0.5$ μm, the BLIP detectivity has been calculated for $T_B = 300$ K and $\eta = 1$.

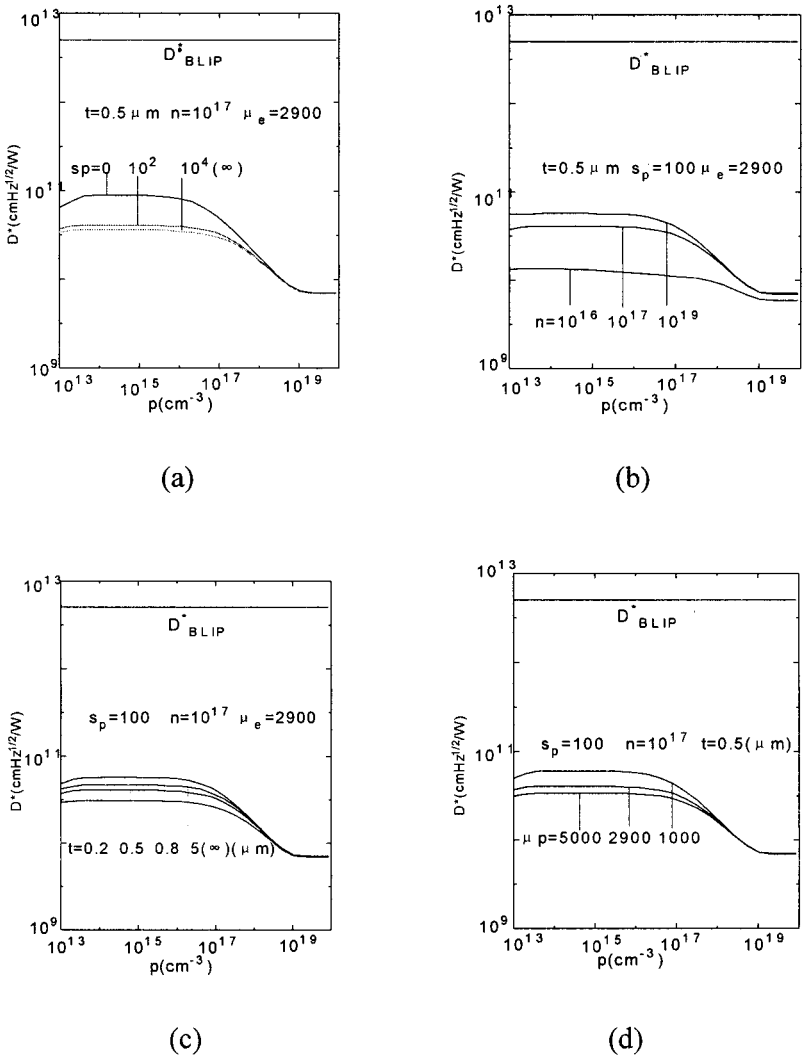

Fig. 8 The calculated detectivity of a GaInAsSb PV detector operated in an *np* structure as a function of the *p*-side carrier concentration *p* and (a) the *n*-side carrier concentration *n*; (b) the *n*-side width *t*; (c) the *n*-side mobility μ_p. In the condition of $S_e=0$, $S_p=100$ m/s, $d=5$ μm, and $\mu_p=240$ cm^2/V s, the BLIP detectivity has been calculated for $T_B=300$ K and $\eta=1$.

1. The optimum material carrier concentration at which the greatest sensitivity of GaInAsSb detectors is obtained depends on the surface recombination velocity. At $S_e=S_p=0$, the *n*- and *p*-side carrier concentrations are both required to be near the intrinsic carrier concentration. As S_e and S_p increase, the optimum carrier concentrations also increase. For example, *p*-side carrier concentration is about 10^{17} cm^{-3}, and the *n*-side carrier concentration is larger than 10^{17} cm^{-3} at $S_e=S_p=100$ m/s (see Fig. 3 and Fig. 4). The surface recombination velocity and carrier concentration are the main influences on the detector sensitivity.
2. The optimum *n*-side width *t* at which the greatest detectivity is obtained also depends on the illuminated-surface recombination velocity. At $S_p=0$, the *n*-side width must be very small ($t\rightarrow 0$). At $S_p=100$ m/s, the optimum *n*-side width is increased to 5 μm. The above results indicate that different S_p require different *n*-side widths.
3. The other parameters, such as the electron mobility μ_e, the hole mobility μ_p, and the *p*-side width *d*, have little effect on the detectivity compared to the surface recombination velocities and carrier concentrations. However, it is hoped to decrease μ_p, μ_e, and *d* to improve the detectivity.

The most disadvantageous structure is that of a detector with high back surface recombination velocity S_e and large *p*-side width *d*. In order to reduce S_e, it is advantageous to use npp^+ structures, since the potential barrier between the *p*- and p^+-type regions limits the flow of minority carriers to the region with more impurities.[9] But the very high ther-

Table 2 Parameters of binary alloys for Eq. (A1).

Alloy	$E_g(T)$ (eV)	Δ	m_e^*	m_h^*	m_s^*	ϵ_r	a_0
GaSb (a_1)	$0.810-3.7810^{-4}T^2/(T+94)$	0.8	0.045	0.49	0.14	15	6.08
GaAs (a_2)	$1.519-5.4010^{-4}T^2/(T+204)$	0.34	0.067	0.45	0.15	10.9	5.65
InSb (a_3)	$0.236-2.9910^{-4}T^2/(T+140)$	0.81	0.014	0.6	0.107	17	6.479
InAs (a_4)	$0.420-2.5010^{-4}T^2/(T+75)$	0.38	0.023	0.41	0.089	14.5	6.058

mal generation of charge carriers to the p^+ region will highly reduce R_0A and D^* of the detector. So utmost care has to be taken with contact and passivation technology to reduce S_e.[19]

It should be noted that the effect of structure on the detectivity is assumed to be determined by the diffusion component of current density, caused by the Auger mechanism. The results will be altered if other mechanisms are considered, such as the radiative mechanism (another diffusion component of the current density) or the generation-recombination mechanism in the depletion region.

In this paper, degeneracy has been neglected in the theoretical analysis of the Auger mechanism in order to simplify the discussion of the performance of the GaInAsSb detector, though a degenerate state exists in material with carrier concentrations up to 10^{21} cm^{-3}.

In conclusion, the theoretical performance of a 2.5-μm $Ga_{0.8}In_{0.2}As_{0.19}Sb_{0.81}$ infrared photovoltaic detector working near room temperature has been analyzed. Through calculating and analyzing the influence of the all material parameters, the optimum performance of the GaInAsSb IR PV detector has been obtained. These results will provide a useful basis for the fabrication of GaInAsSb IR PV detectors.

5 Appendix

The parameters of quaternary alloys such as GaInAsSb have more complicated expressions than those of ternary alloys. In general, these parameters, which are deducible from those of binary and ternary alloys, are obtained by linear interpolation[20]:

$$a=xya_1+x(1-y)a_2+y(1-x)a_3+(1-x)(1-y)a_4, \tag{A1}$$

$$\text{bow}=[(1-x)b_1+xb_2]y(1-y)+[(1-y)b_3+yb_4]x(1-x). \tag{A2}$$

Table 3 Parameters of ternary alloys for Eq. (A2).

	Bowing parameter for	
Alloy	energy bandgap, bow_1	spin-split-off bandgap, bow_2
$InAs_{1-y}Sb_y$ (b_1)	0.58	0.68
$GaAs_{1-y}Sb_y$ (b_2)	1.2	0.51
$Ga_xIn_{1-x}As$ (b_3)	0.436	0.24
$Ga_xAs_{1-x}Sb$ (b_4)	0.415	0.29

The parameters of the binary and ternary alloys that are relevant to quaternary alloys GaInAsSb are shown in Table 2 and Table 3, respectively.

5.1 *Energy Bandgap*

Tian et al.[21] have given a formula for the energy bandgap of GaInAsSb quaternary alloys,

$$E_g(x,y,T)=E_{g_0}(x,y,T)-\text{bow}_1(x,y) \tag{A3}$$

where $E_{g_0}(x,y,T)$ is given by Eq. (A1), for which the corresponding binary-alloy parameters $E_g(T)$ are shown in Table 2. Likewise, $\text{bow}_1(x,y)$ is given by Eq. (A2), for which the ternary-alloy parameters (energy bandgaps) are shown in Table 3.

5.2 *Spin-Split-Off Band*

The formulas for the spin-split-off band are[22]

$$\Delta(x,y)=[1-f(x,y)]\Delta_0(x,y), \tag{A4}$$

$$f(x,y)=\frac{D(x,y)}{E(x,y)}, \tag{A5}$$

$$\frac{1}{E(x,y)}=\frac{1}{3}\left[\frac{2}{E_0(x,y)}+\frac{1}{E_0(x,y)+\Delta_0(x,y)}\right], \tag{A6}$$

$$D(x,y)=\text{bow}_2(x,y), \tag{A7}$$

where $\Delta_0(x,y)$ is obtained from Eq. (A1), and bow_2 from Eq. (A2), for which the relevant parameters are shown in Table 2 and Table 3, respectively.

In this paper, only the energy bandgap and the spin-split-off band are obtained from the revised formulas. The other parameters are obtained directly by linear interpolation [Eq. (A1)].

Acknowledgment

This paper was supported by the National Advanced Material Committee of China (NAMCC).

References

1. B. Zhang, Y. Jin, T. Zhou, H. Jiang, Y. Ning, and S. Li, ''The properties of GaInAsSb/GaSb heterostructures grown by MOCVD and *p*-GaInAsSb/*n*-GaSb photodiodes,'' *Mar. Res. Soc. Symp. Proc.* **415**, 31–26 (1996).

2. J. Benoit, M. Boulou, G. Soulage, A. Joullie, and H. Mani, ''Performance evaluation of GaAlAsSb/GaInAsSb SAM-APDs for high bit rate transmissions in the 2.5 μm wavelength,'' *J. Opt. Commun.* **9**(2), 55–58 (1988).
3. A. Aardvark, G. G. Allogho, G. Bougnot, J. P. R. David, A. Giani, S. K. Haywood, G. Hill, P. C. Klipstein, F. Mansoor, N. J. Mason, R. J. Nicholas, F. Pascal-Delannoy, M. Pate, L. Ponnampalam, and P. J. Walker, ''Devices and desires in the 2–4 μm region based on antimony-containing III–V heterostructures grown by MOVPE,'' *Semicond. Sci. Technol.* **8**(1S), S380–S385 (1993).
4. A. K. Srivastava, J. C. Dewinter, C. Caneau, M. A. Pollack, and J. L. Zyskind, ''High performance GaInAsSb/GaSb p-n photodiodes for the 1.8–2.3 μm wavelength range,'' *Appl. Phys. Lett.* **48**(14), 903–904 (1986).
5. B. Zhang, T. Zhou, H. Jiang, Y. Ning, and Y. Jin, ''GaInAsSb infrared photodetectors prepared by MOCVD,'' *Electron. Lett.* **31**(10), 830–832 (1995).
6. A. Rogalski, R. Ciupa, and W. Larkowski, ''Near room temperature InAsSb photodiodes: theoretical prediction and experimental data,'' *Solid-State Electron* **39**(11), 1593–1600 (1996).
7. A. Rogalski and R. Ciupa, ''Long-wavelength HgCdTe photodiodes: n^+-on-p versus p-on-n structure,'' *J. Appl. Phys.* **77**(4), 3505–3512 (1995).
8. M. B. Reine, A. K. Sood, and T. J. Tredwell, ''Photovoltaic infrared detector,'' Chap. 6 in *Semiconductors and Semimetals*, Vol. 18, R. K. Willardson and A. C. Beer, Eds., pp. 237–, Academic Press, New York (1981).
9. A. Rogalski and J. Rutkowski, ''Effect of structure on the quantum efficiency and R_0A product of lead-tin chalcogenide photodiodes,'' *Infrared Phys.* **22**(2), 199–208 (1982).
10. M. B. Reine, A. K. Sood, and T. J. Tredwell, ''Photovoltaic infrared detector,'' Chap. 6 in *Semiconductors and Semimetals*, Vol. 18, R. K. Willardson and A. C. Beer, Eds., pp. 214–, Academic Press, New York (1981).
11. P. E. Peterson, ''Auger recombination in mercury cadmium telluride,'' Chap. 4 in *Semiconductors and Semimetals*, Vol. 18, R. K. Willardson and A. C. Beer, Eds., pp. 121–155, Academic Press, New York (1981).
12. T. N. Cassalman and P. E. Peterson, ''A comparison of the dominant Auger transition in p-type (Hg,Cd)Te,'' *Solid State Commum.* **33**(6), 615–619 (1980).
13. T. N. Cassalman, ''Calculation of the Auger lifetime in p-type $Hg_{1-x}Cd_xTe$,'' *J. Appl. Phys.* **52**(2), 848–854 (1981).
14. M. Takeshima, ''Auger recombination in InAs, GaSb InP and GaAs,'' *J. Appl. Phys.* **43**(10), 4114–4118 (1972).
15. A. R. Beattie and G. Smith, ''Recombination in semiconductors by a light hole Auger transition,'' *Phys. Status Solidi* **19**(2), 577–586 (1967).
16. A. Rogalski and Z. Orman, ''Band-to-band recombination in $InAs_{1-x}Sb_x$,'' *Infrared Phys.* **25**(3), 551–560 (1985).
17. B. L. Gelmont, ''Auger recombination in diamond-like narrow-gap semiconductors,'' *Phys. Lett.* **66A**(4), 323–324 (1978).
18. A. Rogalski, ''Analysis of the R_0A product in n^+-p $Hg_{1-x}Cd_xTe$ photodiodes,'' *Infrared Phys.* **28**(3), 139–153 (1988).
19. J. Piotrowski, W. Gawron, and Z. Djuric, ''New generation of near room temperature photodetectors,'' *Opt. Eng.* **33**(5), 1413–1421 (1994).
20. R. L. Moon, G. A. Antypas, and L. W. James, ''Bandgap and lattice constant of GaInAsP as a function of alloy composition,'' *Electron. Mater.* **3**(3), 635–644 (1974).
21. Y. Tian, B. Zhang, Y. Jin, T. Zhou, S. Li, Y. Ning, J. Yuan, H. Jiong, and G. Yuan, ''Calculation on relation of energy bandgap to composition and temperature for $Ga_xIn_{1-x}As_{1-y}Sb_y$,'' *Chinese Rare Metals* **15**(3), 172–178 (1996).

Yuan Tian received the BS degree in physics from Jilin University, China, in 1994, and since then, she has been working on her MS and PhD degrees in the program for semiconductor photoelectronic materials and devices at Changchun Institute of Physics, Chinese Academy of Sciences.

Tianming Zhou received the BS degree in physics from the University of Science and Technology of China in 1964. He has been a researcher at Changchun Institute of Physics, Chinese Academy of Sciences, since 1964 and has worked on the growth of semiconductor materials and on optoelectronic devices. His current research interests include the growth and characterization of narrow-bandgap III-V compounds and infrared optoelectronic devices.

Baolin Zhang received the MS degree in semiconductor physics and devices from Jilin University in 1989. He is currently a researcher at Changchun Institute of Physics, Chinese Academy of Sciences. His current research interests include the growth and characterization of III-V compounds by the metal-organic vapor-phase (MOVPE) technique, luminescence from silicon, and optoelectronic devices based on silicon materials. He is a member of the IEEE.

Yixin Jin graduated from the Department of Physics, Peking University, in 1965. Since then he has been with the Changchun Institute of Physics (CIP) of the Chinese Academy of Sciences (CAS). From 1979 to 1981, he worked in the Centre Des Electroniques des Solides, Universite des Sciences et Techniques du Languedoc, France. Meanwhile he received the degree of Docteur de L'Universte en Sciences. His research interests include luminescent materials and physics, preparation and characterization of optoelectronic materials, and functional materials. His current research interest is in photonics.

Yongqiang Ning received the BS degree in electrical engineering from Jilin University in 1987 and the MS degree in electrical engineering from Beijing General Institute for Non-Ferrous Metals in 1990. He has been working in the field of compound semiconductors, especially MOCVD growth of III-V compounds since 1990. He is now pursuing his PhD degree in the field of physics and microcasity lasers at the Changchun Institute of Physics, Chinese Academy of Sciences.

Hong Jiang graduated from the Department of Electrical Science from Jilin University in 1986. She has been working in the field of compound semiconductors, especially MOCVD growth of III-V compounds, since 1986 at the Changchun Institute of Physics, Chinese Academy of Sciences.

Guang Yuan: Biography not available.